[AMERICAN JOURNAL OF SCIENCE, VOL. 274, JANUARY, 1974, P. 61-83]

PREDICTING MINERAL SOLUBILITY FROM RATE DATA: APPLICATION TO THE DISSOLUTION OF MAGNESIAN CALCITES

L. NIEL PLUMMER* and FRED T. MACKENZIE

Department of Geological Sciences,
Northwestern University, Evanston, Illinois 60201

ABSTRACT. The procedure of extrapolating some quantity, measured during dissolution, to infinite time on $(time)^{-1/2}$ plots to predict mineral solubility has been investigated for the dissolution of Iceland spar at 25°C and 0.97 atm CO_2 and used to predict magnesian calcite stability. If kinetic mechanisms of surface reactions do not change and the time to half saturation during dissolution is greater than 10 hours, linear extrapolation of the inflection region on $(time)^{-1/2}$ plots to infinite time is a good estimator of equilibrium conditions. pH and total concentrations of calcium and magnesium in the bulk solution during the dissolution of biogenic magnesian calcites at 25°C and 0.97 atm CO_2 show that Mg-calcite dissolution is initially congruent dissolving the most soluble phase present in the multi-modal skeletal material. The reaction becomes incongruent to calcite and later to 12 mole percent Mg-calcite. The increase of calcium and magnesium ion in the bulk solution follows parabolic rate laws as calcite precipitates. The concentration of calcium ion in the bulk solution decreases during the second incongruent reaction, and the rate with respect to calcium is not parabolic. During the initial congruent dissolution, composition of the dissolving phase was determined from linear slopes on plots of total calcium versus total magnesium in solution. pH data during dissolution were linearly extrapolated to infinite time on $t^{-1/2}$ plots to estimate the congruent equilibrium pH. Log K was computed using the estimated equilibrium pH and composition of the dissolving phase in a FORTRAN IV program. The calculations show that magnesian calcite solubility is maximum at 24 mole percent $MgCO_3$, and the most stable calcite contains about 2 mole percent $MgCO_3$ at 25°C and 1 atm total pressure. The rate studies of magnesium calcites suggest that the stabilization of Mg-calcite skeletal grains in carbonate sediments proceeds in a stepwise manner which accounts for the excellent preservation of Mg-calcite skeletal frameworks in ancient rocks.

INTRODUCTION

In estimating thermodynamic properties of minerals from solubility studies, it is often difficult to determine when a reaction is near equilibrium. Because small changes in concentration over long times are difficult to detect, it is not feasible to determine whether equilibrium has been established from slopes on plots of concentration against time. In addition, many reactions between minerals and aqueous solutions become incongruent before reaching equilibrium, and the resulting rates of dissolution are greatly reduced. Long times may be required to establish heterogeneous equilibria.

This paper investigates a procedure of estimating mineral solubility from the rate at which equilibrium is approached from undersaturation during congruent dissolution. The advantages of predicting mineral solubility from rate data are that (1) the data can be obtained from low temperature-low pressure experiments (where ionic activity coefficients and ionic equilibria are best known), and (2) the reaction does not necessarily have to reach equilibrium. The validity of the procedure is demonstrated for the dissolution of Iceland spar at 25°C and

* Present Address: Department of Geological Sciences, State University of New York at Buffalo, P.O. Box U, Station B, Buffalo, New York 14207

0.97 atm CO_2. The procedure is used to determine the stability of magnesian calcite between 0 and 27 mole percent $MgCO_3$ from the dissolution characteristics of biogenic skeletal material.

INVERSE TIME PLOTS

The method described below was apparently first used by Garrels, Thompson, and Siever (1960) to estimate the solubility of various carbonate minerals. In their experiments, pH was measured as a function of time during the dissolution of the carbonate minerals at 25°C and 0.97 atm CO_2. Garrels, Thompson, and Siever (1960) found that by plotting pH against time$^{-1/2}$, the relationship was nearly linear for long times. Linear extrapolation to infinite time on their plots ($t^{-1/2} = 0$) left little uncertainty in the calculated solubility from the extrapolated congruent equilibrium pH.

An investigation has been made of these empirical plots. Whereas there is no particular significance to the choice of the inverse time function, inverse fractional powers of time give greater separation of data points for long times which facilitate the graphical procedure. Also, the dependent variable is not necessarily restricted to pH or any other logarithmic quantity. The choice of inverse time relationship and dependent variable affects only the scale of the plots. Because $t^{-1/2}$ plots have been widely used (Garrels, Thompson, and Siever, 1960; Bricker, 1965; Kittrick, 1966; Routson and Kittrick, 1971; Weaver, Jackson, and Syers, 1971), they are examined in detail below.

Figure 1 represents schematically the geometry of all $t^{-1/2}$ plots. A dependent variable, Q, which increases with time from a small initial

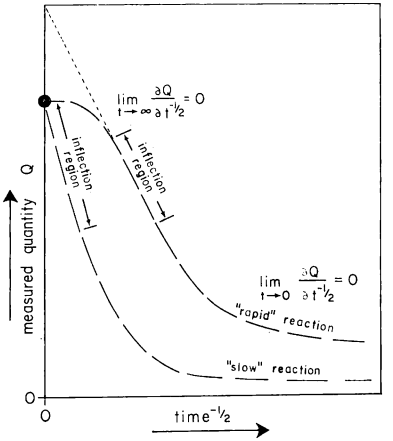

Fig. 1. Comparison of schematic relationships of $t^{-1/2}$ plots for "rapid" and "slow' dissolution. The slope of the measured quantity, Q, approaches zero for very short and very long times. An inflection region between these extremes exists for intermediate times. Extrapolation of the approximately linear inflection region to infinite time estimates a maximum solubility, but as reaction rate is decreased, the extrapolation becomes a better estimator of true solubility.

value and approaches a constant value after long times, is plotted as a function of $t^{-1/2}$ (fig. 1). As time increases, the reaction approaches equilibrium, and thus, the dependent variable changes little as a function of time. Therefore, the slope on $t^{-1/2}$ plots approaches zero as the reaction approaches equilibrium. For small times, $t^{-1/2}$ is large such that the slope is near zero initially, as well. Because Q changes as a function of reaction progress (that is, time), there is an inflection region between the initial and final zero slopes on $t^{-1/2}$ plots. A complete spectrum of these relationships can be demonstrated from theoretical concentration-time curves computed from the congruent dissolution models of Plummer (ms).

Both the zero slope at very large times (Garrels, Thompson, and Siever, 1960, fig. 1B; Bricker, 1965) and the approximately linear inflection region (Garrels, Thompson, and Siever, 1960; Kittrick, 1966; Routson and Kittrick, 1971; Weaver, Jackson, and Syers, 1971) have been extrapolated to infinite time to estimate mineral solubility.

If the slopes are approximately linear and non-zero on $t^{-1/2}$ plots, the experimental data lie in the inflection region (fig. 1). For these cases, linear extrapolation of the inflection region to infinite time predicts a solubility greater than the true solubility (fig. 1) as was pointed out by Garrels, Thompson, and Siever (1960).

In general, however, as the surface area to volume ratio in dissolution experiments is decreased, the linear portion of the inflection region on $t^{-1/2}$ plots is extended and shifted toward infinite time, while the slope, $dQ/d(t^{-1/2})$, becomes more negative (fig. 1). The shift in the linear portion of the inflection region toward infinite time results in a closer approximation of the true equilibrium value of Q (fig. 1). The decrease in slope on $t^{-1/2}$ plots introduces more uncertainty in extrapolation to infinite time, and the resulting error is a function of the precision of the analytical data.

These relationships are demonstrated in a series of experiments (Plummer, ms) on the dissolution of Iceland spar crystals at 25°C in CO_2 saturated solutions at 1 atm total pressure in which the surface area to bulk solution volume ratio ranged from 20 to 11,200 $cm^2\ l^{-1}$. In the experiments surface area was estimated from the weight of sized material assuming rhombohedral particle shape of dimensions equal to the mean sieve size. The reactions were followed by measurement of pH in the stirred bulk solutions as a function of time similar to the procedure of Garrels, Thompson, and Siever (1960).

It is seen in figure 2 that as the surface area to solution volume ratio in the Iceland spar experiments is reduced, linear extrapolation of the inflection region on $t^{-1/2}$ plots to infinite time becomes a good estimator of the equilibrium pH (pH = 6.02). The precision of the pH measurements (± 0.02 pH) is such that little error is introduced by extrapolating data of more negative slopes to infinite time. It is estimated that if the surface area to solution volume ratio is maintained

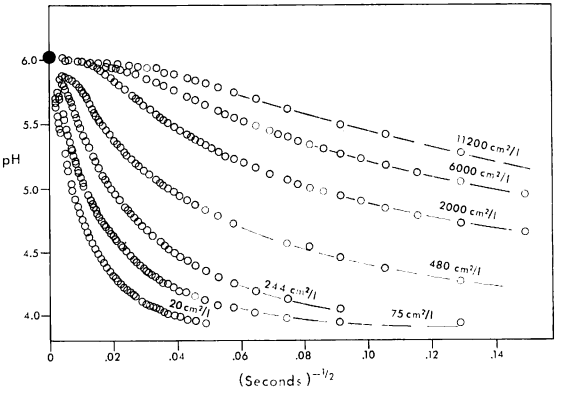

Fig. 2. pH during the dissolution of Iceland spar as a function of $t^{-1/2}$ for surface area to volume ratios of 20 cm^2 l^{-1} to 11,200 cm^2 l^{-1}. By decreasing the surface area to volume ratio to approximately 200 cm^2 l^{-1}, or less, linear extrapolation of the inflection region to infifinite time predicts the true equilibrium pH (6.02).

less than approximately 200 cm^2 l^{-1} during the dissolution of Iceland spar at 25°C and 0.97 atm CO_2, the extrapolation to infinite time on $t^{-1/2}$ plots estimates the true solubility. Obviously, the rates of dissolution vary between differing minerals, and therefore, the limiting surface area to volume ratio differs among minerals. As a general rule, however, if the surface area to volume ratio is adjusted so that the time required for the dissolution reaction to reach half saturation is no less than approximately 10 to 12 hours, the procedure predicts the true solubility.

It is seen in figure 2 that not all pH versus $t^{-1/2}$ curves for Iceland spar dissolution appear to approach the equilibrium value (compare the 480 cm^2 l^{-1} run). Actually, there are abrupt changes in curvature in all the runs that approached equilibrium (480, 2000, 6000, and 11,200 cm^2 l^{-1} runs). It is interesting that these changes are approximately coincident with pH 5.85 which is the value observed for a change in reaction mechanism to a slower, higher order reaction at the calcite surface (Plummer, ms). This value indicates the Δ pH of the change in these experiments to be approximately 0.17, near that reported by Morse and Berner (1972) for a different experimental condition.

Thus, it is seen that in addition to its dependency upon the surface area to volume ratio, the inverse time plot technique can only be applied to that part of a heterogeneous reaction that is controlled by a single kinetic process.

The example given above for Iceland spar demonstrates the validity of $t^{-1/2}$ plots. However, the importance of this method is not in its application to minerals that dissolve congruently, because their solubilities can be measured directly. The significance of the procedure is in estimating the congruent solubility of minerals that dissolve incongruently before reaching equilibrium. When these reactions become incongruent, the rate of dissolution is greatly decreased, and it becomes

difficult to determine when equilibrium has been obtained. For this class of reactions, the application of inverse time plots to initial congruent reaction segments is a valuable technique in predicting mineral solubility.

We will now look at the dissolution reaction paths of Mg–calcites before applying the inverse time plot techniques to determination of their solubilities.

APPLICATION TO MAGNESIAN–CALCITE DISSOLUTION

To apply the inverse time plot technique to estimating Mg–calcite solubility, the stoichiometry of the dissolution reaction must be determined; that is, the composition of the dissolving phase must be known, and for the experiments described below, it must be known that the reaction is congruent. Consequently, careful observation of the composition of the bulk solution during dissolution is necessary.

If the calcium/magnesium ratio in the bulk solution remains constant during dissolution, then congruent dissolution of a single phase is occurring according to the reaction

$$Ca_{(1-x)}Mg_{(x)}CO_3 \rightarrow (1-x)Ca^{++} + (x)Mg^{++} + CO_3^{--} \qquad (1)$$

where the mole fraction of magnesium in the dissolving phase, x_{Mg}, is

$$x_{Mg} = \frac{1}{\frac{Ca}{Mg} + 1} \qquad (2)$$

and Ca/Mg is the ratio of the total molarity of calcium to the total molarity of magnesium in solution.

Dissolution experiments have been made with hydrothermally prepared Mg–calcites (Williams, written commun., 1972). However, interpretation of these data is difficult because (1) there was insufficient sampling of solution composition during runs, (2) complexing was not considered in calculating ionic activities, (3) the reactant material possibly was multi-phase, and (4) insufficient material was used in the dissolution experiments to warrant an assumption of constant surface area.

Biogenic Mg–calcite material, collected from Bermuda, was used in the authors' experiments. Because some biogenic materials are known to contain more than one Mg–calcite phase (Moberly, 1968, 1970; Milliman, Gastner, and Muller, 1971), as well as brucite (Schmalz, 1965; Weber and Kaufman, 1965) and perhaps protodolomite (Schroeder, Dwornik, and Papike, 1969), the dissolution at 25°C and 0.97 atm CO_2 was carefully followed by measurement of pH and total concentrations of calcium, magnesium, and alkalinity in the bulk solution to determine the reactions taking place. Calcium and magnesium were measured by EDTA titration, and alkalinity by potentiometric titration and Gran plots (Stumm and Morgan, 1970). The experimental procedure was similar to that described for the dissolution of Iceland spar (Plummer,

in preparation). The distribution of aqueous species was calculated in a Fortran IV program using the data of table 1. Charge balance computed from the experimental data agrees within 2 percent. In the discussion that follows, a general reference to "calcite" can imply as much as 4 mole percent $MgCO_3$ in solid solution. The designation "Mg–calcite" implies more than 4 mole percent $MgCO_3$ in the composition.

The data obtained for the dissolution of the alga *Amphiroa rigida* are representative of all the Mg–calcite dissolution data collected. In the experiment, 6.500 g of *Amphiroa r.*, sized between 44 and 74 microns, were placed in 650 ml of distilled water maintained at 25°C. In this experiment agitation was provided by a shaker table, and CO_2 was continuously bubbled through the solution at 0.97 atm.

The gross characteristics of the irreversible reaction can be seen in a plot of the total concentrations of calcium and magnesium in the bulk solution as a function of time (fig. 3). There are initially rapid increases in both calcium and magnesium in the bulk solution. After

TABLE 1

Log equilibrium constants at 25°C and 1 atm pressure

$CaCO_3^\circ = Ca^{++} + CO_3^{--}$	−3.1	1.
$MgCO_3^\circ = Mg^{++} + CO_3^{--}$	−3.40	1.
$CaHCO_3^+ = Ca^{++} + HCO_3^-$	−1.225*	2.
$MgHCO_3^+ = Mg^{++} + HCO_3^-$	−0.90	1.
$H_2O = H^+ + OH^-$	−14.00	3.
$H_2O + CO_2 = CO_2 = H_2CO_3$	−1.4635	4.
$H_2CO_3 = H^+ + HCO_3^-$	−6.3519	4.
$HCO_3^- = H^+ + CO_3^{--}$	−10.329	5.

1. Lafon (ms).
2. Written communication (1972) from C. L. Christ pertaining to the work of P. B. Hostetler, R. M. Siebert, and C. L. Christ.
3. Helgeson (1969).
4. Harned and Davis (1943).
5. Harned and Scholes (1941).

* The aqueous model for the system $CaO–CO_2–H_2O$ in question. Although three determinations of the dissociation constant of $CaHCO_3^+$ are in close agreement (Greenwald, 1941; Nakayama, 1968; Christ, written commun., 1972), calcite solubility computed from the observed equilibrium pH of 6.02 (Plummer, 1972) at 0.97 atm CO_2 and 25°C assuming the presence of $CaHCO_3^+$ (9.8 mmoles/l) is much larger than the observed solubility (9.1 mmoles/l) as was pointed out by Langmuir (1968). If the maximum P_{CO_2} obtained by bubbling pure CO_2 through pure water is about 0.92 atm (rather than 0.97 atm), computed solubilities of calcite are then in agreement with observed values assuming the presence of $CaHCO_3^+$. However, there is no evidence to support partial pressures of CO_2 as low as 0.92 atm. Also, if the P_{CO_2} were as low as 0.9 atm, the pH of the solution at 1 atm total pressure and 25°C would be near 3.93. The observed pH (3.91; Garrels, Thompson, and Siever, 1960) is in agreement with that calculated at 0.97 atm CO_2. Because of the uncertainty in the aqueous model, Mg–calcite equilibrium ion activity products (table 3) have been computed assuming (1) $P_{CO_2} = 0.97$ atm and $CaHCO_3^+$ present, (2) $P_{CO_2} = 0.92$ atm and $CaHCO_3^+$ present, and (3) $P_{CO_2} = 0.97$ atm and $CaHCO_3^+$ absent. Because (1) measured total molalities of calcium during the dissolution of magnesian calcites are in close agreement with values computed assuming $P_{CO_2} = 0.97$ atm and the absence of $CaHCO_3^+$, and (2) there is no evidence for CO_2 partial pressures as low as 0.92 atm, Mg–calcite stability data have been computed (table 3) assuming the absence of $CaHCO_3^+$ at 0.97 atm CO_2.

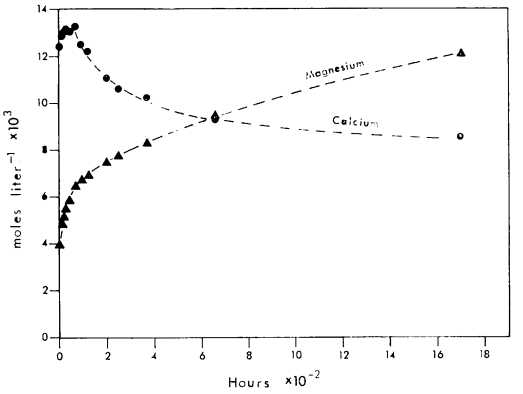

Fig. 3. Total concentrations of calcium and magnesium in the bulk solution as function of time during the dissolution of *Amphiora r.* The reaction becomes incongruent to calcite resulting in a decrease in the calcium concentration in the bulk solution after 70 hours.

approximately 70 hrs, the calcium concentration begins to decrease while the magnesium concentration continues to increase throughout the reaction. This is evidence that the reaction becomes incongruent, and a calcium-rich phase forms. If magnesium also occurs in the incongruent phase, the net stoichiometry of the reaction(s) leaves an excess magnesium content in solution. A plot of total calcium against total magnesium in the bulk solution shows three distinct changes in slope which represent important events during the irreversible reaction (fig. 4).

Congruent dissolution.—Stage 1 (fig. 4) is represented by a linear relationship between calcium and magnesium. Because this initial re-

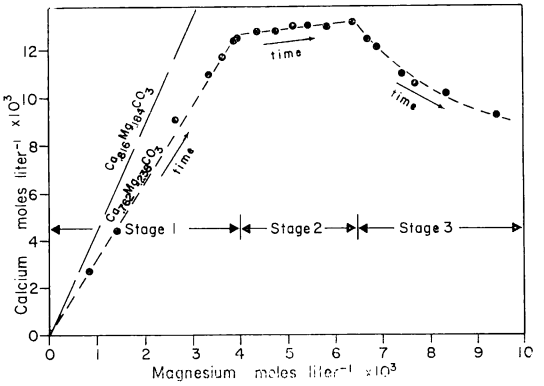

Fig. 4. Reaction stages during the dissolution of *Amphiroa r.* defined by slope changes on a plot of total calcium versus total magnesium in the bulk solution. Stage 1 is the congruent dissolution of the most soluble magnesian calcite in the multimodal mixture. Although *Amphiroa r.* has a mean composition (assuming a single phase) of 18.4 mole percent $MgCO_3$, the algae dissolves as 23.8 mole percent $MgCO_3$. The reaction becomes incongruent to calcite in stage 2 with nucleation on grain surfaces. In stage 3 precipitation from the bulk solution occurs as well.

action segment is linear on similar plots for all the dissolution data collected, congruent dissolution of a single phase is occurring. For the dissolution of *Amphiroa r.*, stage 1 corresponds to the congruent dissolution of 23.8 mole percent magnesium calcite.

However, from all the data collected, the composition of the dissolving phase during stage 1 is always more Mg-rich than that suggested by the mean and modal compositions as determined by bulk chemical analysis and X-ray diffraction techniques, respectively. Bulk chemical analysis indicates *Amphiroa r.* to be 18.4 mole percent $MgCO_3$ (assuming the alga to be a single Mg–calcite phase). The displacement of the (211) calcite peak on X-ray diffractograms indicates the modal composition to be approximately 19 mole percent $MgCO_3$.

Microprobe analysis of biogenic Mg–calcites show the composition to be variable within a single specimen (Moberly, 1968, 1970). Milliman, Gastner, and Muller (1971) show that the shift in the calcite diffraction peak only indicates the modal phase in the biogenic skeletal material. They interpret the asymmetry of the diffraction patterns as evidence for the presence of multiple Mg–calcite phases within the skeleton. This interpretation is supported by the dissolution data as well. In table 2 the modal composition, approximate range in composition, and the composition of the dissolving phase are compared for various biogenic Mg–calcites. The modal composition and approximate range in composition within each specimen were determined from the 2θ peak position of the (211) reflection and the peak width, respectively, using the X-ray diffraction data of Goldsmith, Graf, and Heard (1961). The composition of the dissolving phase was determined from the slope of the initial reaction segment on total calcium versus total magnesium plots and equation (2). Table 2 shows that the composition of the dissolving phase corresponds to the composition of the most Mg-rich calcite in

TABLE 2

Comparison of the composition of biogenic Mg–calcites with the initial congruent composition*

Range**	Mode**	Composition of Dissolving Phase	Specimen
0-7	1	6.9	*Ostrea sp.*
0-10	2	10.4	"Barnacle"
2-13	6	12.7	*Diadema* spine
6-18	11	17.9	*Diadema* test
10-19	16	19.2	"Sand Dollar"
9-32	17	23.6	*Goniolithon sp.*
6-34	19	23.8	*Amphiroa r.*
6-34	19	24.4	*Amphiroa r.*
11-32	20	24.7	*Amphiroa f.* (1)
11-32	20	26.7	*Amphiroa f.* (2)

* All data are in mole percent $MgCO_3$

** Analysis by X-ray diffraction using the data of Goldsmith, Graf, and Heard (1961).

the mixture for all material in the compositional range of 0 to 20 mole percent $MgCO_3$. Many of the biogenic Mg–calcites range up to 34 mole percent $MgCO_3$ (table 2), but for these, the composition of the dissolving phase is approximately 24 mole percent $MgCO_3$. One specimen, *Amphiroa fragilissima,* apparently dissolved as 24.7 mole percent $MgCO_3$ initially and then changed abruptly dissolving 26.7 mole percent $MgCO_3$ (fig. 5).

These observations can be explained, if the composition of the dissolving phase during stage 1 is that of the most soluble Mg–calcite in the mixture. If this assumption is correct, the dissolution data suggest that the solubility of Mg–calcites increases to a maximum at about 24 mole percent $MgCO_3$. In the example of *Amphiroa f.* (fig. 5), the most soluble phase in the mixture, 24.7 mole percent $MgCO_3$, was apparently not in excess, and when consumed in the reaction, the next most soluble phase, 26.7 mole percent $MgCO_3$ began dissolving. This initial slope corresponds to the dissolution of approximately 0.08 g of *Amphiroa f.* which is less than 1 percent by weight of the total material used in the experiment. If the entire surface was dissolving, a layer approximately 10^{-6} cm thick was dissolved during the dissolution of the 24.7 mole percent $MgCO_3$ fraction of *Amphiroa f.* It will be shown later that the solubility of Mg–calcites does indeed go through a maximum at approximately 24 mole percent $MgCO_3$.

The stepwise shift in slope during the dissolution of *Amphiroa f.* (fig. 5) supports the evidence of Moberly (1968, 1970) that biogenic Mg–calcites are discrete multi-modal mixtures; that is, they are not a continuous spectrum of compositions.

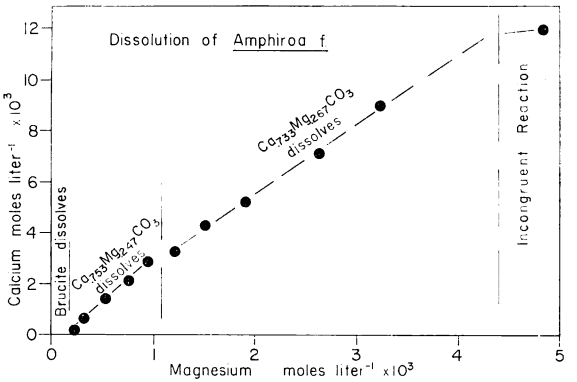

Fig. 5. Characteristics of the congruent dissolution of *Amphiroa f.* defined by a plot of total calcium versus total magnesium in the bulk solution. First to dissolve is a small amount of brucite initially present on the grain surfaces. After the consumption of the brucite, the reaction is dominated by the congruent dissolution of the most soluble phase, 24.7 mole percent $MgCO_3$, on the surface. This phase is apparently consumed in the reaction, and the next most soluble phase, 26.7 mole percent $MgCO_3$, dissolves. The reaction was terminated after becoming incongruent to calcite (stage 2).

An explanation for the stepwise dissolution of a single most soluble phase in a mixture of biogenic Mg–calcites requires the solution at the mineral-aqueous solution interface to be near equilibrium with the most soluble Mg–calcite in the organic matrix, such that Mg–calcites of lesser solubility do not dissolve. A compositional map of the surface of a biogenic Mg–calcite taken from Moberly (1970) is shown in figure 6. This map shows the distance between discrete Mg–calcite phases within a single grain to be 2-4 $\times$ 10^{-3} cm which is approximately the distance commonly reported for the thickness of "diffusion layers" (Bircumshaw and Riddiford, 1952). Thus, solutions in equilibrium with discrete patches on grain surfaces could overlap spatially, preventing adjacent Mg–calcite domains of lesser solubility from dissolving. However, because the kinetics of calcite dissolution between pH 4 and 6 (Morse and Berner, 1972; Plummer, in preparation) may be slower than that expected for "diffusion-controlled" reactions, we have little reason to suspect that the dissolution kinetics of Mg–calcites in our experiments are very different from calcite (although this has not been confirmed). If Mg–calcite dissolution is slower than "diffusion-control", one might expect subsaturated solutions near the surfaces of mineral grains. It is likely, however, that the transport of reaction products from a high porosity skeletal framework surface into bulk solution would be retarded by buildup of residual organic matrix on the surface, which would enhance the likelihood of surface concentrations near equilibrium with the most soluble phase. To explain the observations in stage 1, we need only to conclude that the rate of transport of reaction products from surface interstices through a residual organic matrix on the surface is slower than the rate of dissolution of magnesian calcite.

The fact that the distance between discrete domains of Mg–calcites within the matrix of *Amphiroa f.* may be three orders of magnitude greater than the thickness of the layer removed from the surface during the dissolution of the 24.7 mole percent $MgCO_3$ fraction (fig. 5) supports

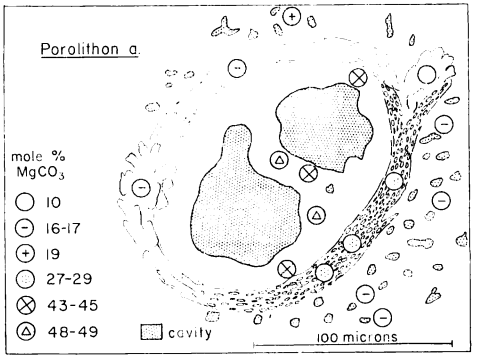

Fig. 6. Electron microprobe analysis of *Porolithon aequinoctiale.* Size of symbol is area analyzed by electron beam. The distance between discrete patches of magnesian calcite is suggested to be approximately 20 to 40 microns or less. From Moberly (1970, p. 116, fig. 3).

the assumption that the most soluble fraction was not in excess on the grain surfaces.

Several investigators have suggested that brucite occurs in magnesian calcite algae of greater than 20 to 25 mole percent $MgCO_3$ (Schmalz, 1965; Weber and Kaufman, 1965; Moberly, 1970; Milliman, Gastner, and Muller, 1971). The dissolution data for the Mg–calcite algae also suggest the presence of brucite. Much of the data show that the first mineral to dissolve is a nearly pure magnesium phase (fig. 5). All this phase, presumably brucite, in contact with the bulk solution appears to be consumed in an initially rapid reaction and does not affect the later reaction path.

Incongruent dissolution.—From the observations presented below, it seems most likely that stage 2 is initiated by the growth of calcite on grain surfaces. Calculations from the activities of species in solution indicate that the bulk solution is 2.2 times saturated with respect to calcite at the beginning of stage 2. This is about half that predicted by Wollast (1971) for heterogeneous nucleation of calcite. Because some calcium continues to enter the bulk solution during stage 2 (fig. 4), the amount of calcite precipitated must not be in the same stoichiometric proportions as that of Mg–calcite dissolved. During stage 3, calcite precipitates from the bulk solution causing a decrease in the calcium concentration approaching calcite saturation (fig. 4).

The reaction path for the experimental data on the dissolution of *Amphiroa r.* is plotted on a log $a_{Ca^{++}}/a^2_{H^+}$ versus log $a_{Mg^{++}}/a^2_{H^+}$ diagram calculated at 25°C and 1 atm CO_2 taking the activity of water to be unity (fig. 7). The initial reaction path passes from undersaturation to supersaturation with respect to calcite. There is an abrupt change in slope in the reaction path with the initiation of stage 2, after which the path parallels the calcite equilibrium line at 2.2 times calcite saturation. Owing to the close overlap of the experimental data, not all points during stages 2 and 3 are shown on figure 7. With the initiation of stage 3, the quantity log $a_{Ca^{++}}/a^2_{H^+}$ decreases from 10.16 to 10.12 as the bulk solution slowly approaches calcite saturation. When terminated, the reaction was approaching a metastable Mg–calcite—calcite equilibrium. But if allowed to continue, the reaction would greatly supersaturate with respect to magnesite and dolomite before reaching the metastable equilibrium state.

Comparison of X-ray diffraction patterns of the initial reactant *Amphiroa r.* with the reacted material after 70 days (fig. 8) shows the presence of the incongruent calcite with the reacted material. The asymmetry toward more Mg-rich calcite in the starting material is reduced somewhat in the reacted material. This shift in peak symmetry demonstrates that the higher Mg-calcite portion of *Amphiroa r.* dissolved incongruently to calcite.

Many incongruent reactions can be modeled as diffusion of reactants and products through low porosity product layers growing on the mineral surface by

$$\frac{dC_i}{dt} = kt^{-1/2} \tag{3}$$

which is the parabolic rate law (Jost, 1952; Crank, 1956; Wollast, 1967; Helgeson, 1971; Luce, Bartlett, and Parks, 1972) where C_i is the concentration of the i^{th} species in the bulk solution, t is time, and k is the parabolic rate constant which is a function of the molecular diffusion coefficient for the i^{th} species, surface area of the reactant mineral, porosity of the product layer, volume of the bulk solution, and stoichiometry of the incongruent reaction. Integration of equation (3) gives

$$C_i = 2kt^{1/2} \tag{4}$$

which indicates that for incongruent reactions obeying the parabolic rate law, concentration in the bulk solution is directly proportional

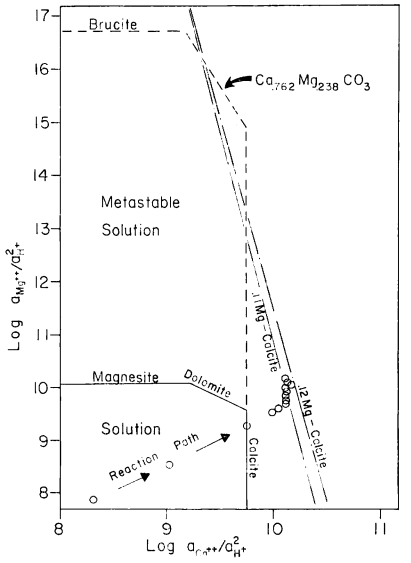

Fig. 7

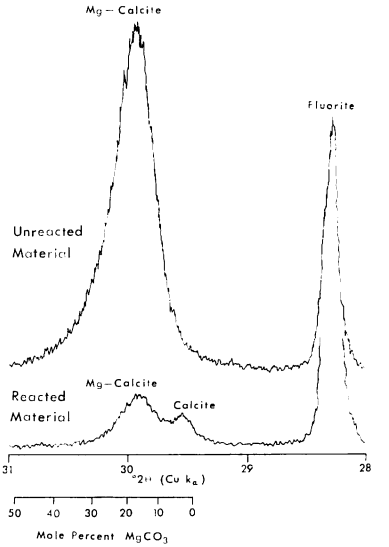

Fig. 8

Fig. 7. Saturation diagram for the system CaO–MgO–CO_2–H_2O at 25°C and 1 atm CO_2 total pressure showing the measured reaction path for the dissolution of *Amphiroa r.* Calcite precipitation is indicated by an abrupt change in slope of the reaction path to a line parallel to the calcite equilibrium line at 2.2 times calcite saturation. When terminated, the bulk solution was near equilibrium with 11 to 12 mole percent magnesian calcite. Computed from the data of table 3 and Robie and Waldbaum (1968).

Fig. 8. Comparison of X-ray diffraction patterns of initial reactant *Amphiroa r.* with reacted material after 70 days. The presence of low Mg–calcite in the reacted material indicates an incongruent reaction. The assymetry toward more Mg-rich calcites in the starting material is reduced in the reacted material indicating that the higher Mg–calcite portion of *Amphiroa r.* dissolved incongruently to calcite.

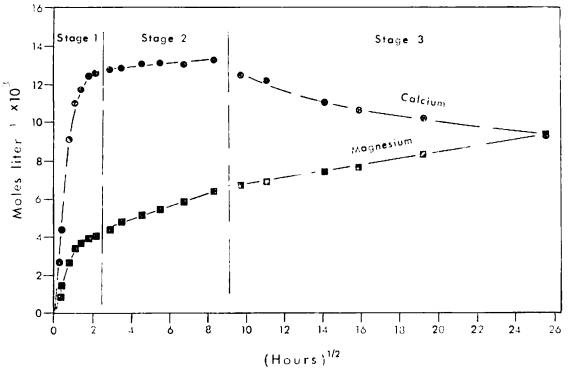

Fig. 9. Total concentrations of calcium and magnesium in the bulk solution as a function of square root of time during the dissolution of *Amphiroa r.* Three reaction stages (fig. 4) are again defined by breaks in slope. The magnesium concentration in the bulk solution shows a linear relationship with the square root of time in stages 2 and 3 indicating that parabolic rate laws are obeyed. Stage 3 corresponds to the precipitation of approximately 11.7 mole percent magnesian calcite.

to the square root of time. Thus, evaluation of slopes on plots of concentration against the square root of time is particularly useful in identifying incongruent reactions and defining parabolic rate constants.

From figure 9 it is evident that plots of total concentrations of calcium and magnesium in the bulk solution versus square root of time during stage 1 are non-linear which is further permissive evidence for congruent dissolution in stage 1. The slopes for calcium and magnesium are both linear during stage 2 indicating that their release to the bulk solution during stage 2 is controlled by diffusion through a product layer. While the release of magnesium to the bulk solution is parabolic in stage 3, the calcium concentration decreases in the bulk solution, and its rate of removal is not parabolic (fig. 9). Because the slope is linear and decreases for the magnesium release to the bulk solution between stages 2 and 3, the reaction must be incongruent to a more magnesium-rich phase. The additional points after 70 days, not included in figure 9, further support these conclusions.

Evaluation of the change in slope between stages 2 and 3 gives information on the composition of the phase precipitating during stage 3. This procedure can be demonstrated by correcting the parabolic rate constant in the integrated form of the parabolic rate law (eq 4) for the net stoichiometry of the incongruent reaction

$$C_i = 2(1 - n_i^*)k't^{1/2}. \tag{5}$$

In equation (5), k′ is the parabolic rate constant divided by $1 - n_i^*$ which is a term for the net stoichiometry of the incongruent reaction in which n_i^* is defined by

$$n_i^* = \frac{\nu_i \text{ (product)}}{\nu_i \text{ (reactant)}} \tag{6}$$

where ν_i is the stoichiometric coefficient for the i^{th} component in the reactant or product mineral. If none of the i^{th} component precipitates in the product layer, ν_i and thus, n_i^* is zero, and the slope on C_i versus $t^{1/2}$ plots is k′. If all of the i^{th} components in the reactant precipitates in the product, n_i^* is one, and thus, the slope on C_i versus $t^{1/2}$ plots is zero (eq 5). All other incongruent reactions of intermediate stoichiometry have slopes between k′ and zero on C_i versus $t^{1/2}$ plots.

Although the true composition of the calcite formed in stage 2 is not known, little error is introduced in the calculations below by assuming the mineral to be pure calcite. Therefore, n_{Mg}^* in equation (6) is approximately zero, and the slope of the magnesium data on figure 9 during stage 2 defines the parabolic rate constant, k′, for the dissolution of *Amphiroa r.* from equation (5) to be 3.3×10^{-4} moles l^{-1} $sec^{-1/2}$. The slope of the magnesium data during stage 3 (fig. 9) is 1.68×10^{-4} moles l^{-1} $sec^{-1/2}$, and dividing that slope, $(1 - n_{Mg}^*)k'$, by k′ defines n_{Mg}^* during stage 3 to be 0.491. Because ν_{Mg} for the reactant *Amphiroa r.* is 0.238, the composition of the product magnesium calcite during stage 3 is $Ca_{0.883}Mg_{0.117}CO_3$, as calculated from equation (6).

We can further demonstrate the above observations by writing possible reactions for each stage during dissolution. The reactions are presented below only to demonstrate mass balance relations and in no way imply kinetic mechanisms of dissolution. It has been shown above that the first stage in the reaction is the congruent dissolution of the most soluble Mg–calcite in the multi-modal skeletal material which for *Amphiroa r.* is 23.8 mole percent magnesian calcite. Stage 1 can be represented by

$$Ca_{0.762}Mg_{0.238}CO_3 \rightarrow 0.762Ca^{++} + 0.238Mg^{++} + CO_3^{--}. \qquad (7)$$

Calcite nucleates on grain surfaces during stage 2, and the release of calcium and magnesium into the bulk solution obeys parabolic rate laws. Because calcium continues to increase in the bulk solution during stage 2, there must be an excess calcium content in the incongruent reaction, and because a more calcium-rich product is forming, the incongruent reaction is similar to

$$2Ca_{0.762}Mg_{0.238}CO_3 \rightarrow 1.4Ca_{0.98}Mg_{0.02}CO_3 + 0.152Ca^{++} + 0.448Mg^{++} + 0.6CO_3^{--}; \qquad (8)$$

if, for example, the calcite precipitated in stage 2 contains 2 mole percent $MgCO_3$. According to equations (7 and 8), the calcium to magnesium ratio of the ions entering the bulk solution between stages 1 and 2 changes from 3.2 to 0.33 which accounts for the decrease in slope on the plot of observed calcium versus magnesium (fig. 4). During stage 3, the calcium concentration decreases in the bulk solution indicating that a calcium-rich phase is growing from the bulk solution. The composition of this phase is estimated to be near $Ca_{0.883}Mg_{0.117}CO_3$. Because the rate of increase of magnesium in the bulk solution during stage 3 follows a parabolic rate law, it is probable that the second incongruent Mg–calcite

precipitates within the product layer. To assume that this Mg–calcite phase is precipitating from the bulk solution requires the rate of removal of magnesium from the bulk solution to follow a parabolic rate law, which is unlikely. Stage 3 can be represented by

$$0.152Ca^{++} + 0.448Mg^{++} + 0.6CO_3^{--}{}_{(\text{stage 2})} + 0.378Ca^{++}{}_{(\text{bulk})} \rightarrow 0.6Ca_{0.883}Mg_{0.117}CO_3 + 0.378Mg^{++}. \quad (9)$$

Although it is not confirmed, it is implied by equation (9) that both calcite and approximately 12 mole percent $MgCO_3$ calcite precipitate simultaneously in the product layer during stage 3.

With this understanding of biogenic Mg–calcite dissolution, we can now apply the $t^{-1/2}$ relationship developed previously to congruent dissolution data and estimate Mg–calcite stability.

MG–CALCITE STABILITY

To determine the stability of Mg–calcites from $t^{-1/2}$ relationships, the composition of the dissolving phase was obtained from the slope on total calcium versus total magnesium plots for stage 1 using equation (2). Surface area was estimated by graphical means to be less than 200 cm^2 l^{-1} in the experiments, and pH was measured continuously during the dissolution at 25°C and 0.97 atm CO_2. The pH data were plotted as a function of time $^{-1/2}$ and linearly extrapolated to infinite time to estimate the equilibrium value. From the estimated equilibrium pH, P_{CO_2}, and the data in table 1, equilibrium ion activity products (table 3) were computed for each phase. In computing the equilibrium constants, activity coefficients of charged species were computed from the extended Debye-Huckel equation using ion size data from Butler (1964), and assuming $å_{MHCO_3^+} = 4.0$, and values for the A and B parameters from Helgeson (1967). Activity coefficients of neutral species were computed from the relation $\gamma_i^\circ = 10^{0.1I}$, where I is ionic strength. Convergence on the equilibrium distribution of species is within 10^{-9} ionic strength. Although it is felt that the stability data obtained are near the true values, the extrapolated values represent maximum solubility limits. Two examples of pH versus $t^{-1/2}$ which demonstrate that the plots are linear as $t^{-1/2}$ approaches zero are shown for inspection in figure 10.

The maximum log K data obtained by extrapolation to infinite time are plotted as a function of mole percent $MgCO_3$ in figure 11. It is seen that Mg–calcites go through a maximum solubility at approximately 24 mole percent $MgCO_3$, and the most insoluble Mg–calcite contains about 2 mole percent $MgCO_3$.

Chave and others (1962) and Land (1967) report "steady state" pH measurements for the dissolution of Mg–calcites at 25°C and 0.97 atm CO_2. These data provide minimum solubilities because the steady state pH measured represents not the congruent solubility but a constant pH owing to buffering by the incongruent precipitation of calcite (stage 2). The composition of the dissolving phase reported by Chave and

others (1962) and Land (1967) is also a minimum estimate, because it was determined from bulk chemical analysis assuming that the skeletal material is a single phase. Computed Mg–calcite free energies of formation ($\Delta G_f°$) from steady state pH data (Winland, 1969) are too negative.

The values computed from our data suggest that some calcites of Chave and others (1962) (2-3 mole percent $MgCO_3$) may have dissolved congruently, and if we accept their data, Mg–calcite solubility passes through a minimum around 2 to 3 mole percent $MgCO_3$. However, this conclusion is inconsistent with the experimental work of Goldsmith and Heard (1961) on the system $CaCO_3$–$MgCO_3$, if extrapolation of their data to 25°C is warranted.

The Gibbs free energies of formation of magnesium calcites at 25°C and 1 atm total pressure have been computed from the log K data using the standard free energies of formation for Ca^{++} and Mg^{++} of

TABLE 3

Estimated stability of Mg–calcites at 25°C and 1 atm total pressure

Composition	pH*	Log K**	Log K***	Log K†	Kcal/mole†† $\Delta G_f°$	Kcal/mole†† ΔG_m	Activities in solid solution††,£ a_{CaCO_3}	Activities in solid solution††,£ a_{MgCO_3}	Source
$CaCO_3$ (Calcite)	6.02	−8.45	−8.49	−8.412	−269.94	0	1.00	——	‡
$Ca_{(0.980)}Mg_{(0.020)}CO_3$	6.02	−8.49	−8.53	−8.45	−269.53	−0.07	0.98	0.01	§
$Ca_{(0.970)}Mg_{(0.030)}CO_3$	6.00	−8.56	−8.60	−8.53	−269.39	−0.17	0.85	0.02	§
$Ca_{(0.931)}Mg_{(0.069)}CO_3$	6.10	−8.33	−8.37	−8.29	−268.16	0.14	1.56	0.08	‡
$Ca_{(0.896)}Mg_{(0.104)}CO_3$	6.24	−7.98	−8.02	−7.94	−266.84	0.62	3.72	0.31	‡
$Ca_{(0.873)}Mg_{(0.127)}CO_3$	6.29	−7.86	−7.90	−7.82	−266.13	0.78	5.00	0.53	‡
$Ca_{(0.821)}Mg_{(0.179)}CO_3$	6.44	−7.49	−7.53	−7.43	−264.39	1.29	12.29	1.99	‡
$Ca_{(0.808)}Mg_{(0.192)}CO_3$	6.49	−7.37	−7.40	−7.30	−263.90	1.47	16.64	2.96	‡
$Ca_{(0.764)}Mg_{(0.236)}CO_3$	6.55	−7.23	−7.26	−7.16	−262.67	1.65	22.98	5.36	‡
$Ca_{(0.756)}Mg_{(0.244)}CO_3$	6.55	−7.23	−7.27	−7.16	−262.48	1.64	22.72	5.54	‡
$Ca_{(0.733)}Mg_{(0.267)}CO_3$	6.52	−7.32	−7.36	−7.26	−262.07	1.51	18.15	4.97	‡

* Estimated equilibrium pH at 25°C in CO_2 saturated solutions at 1 atm total pressure.

** Estimated log equilibrium ion activity product (log K) computed from pH and phase composition at P_{CO_2} = 0.97 atm using the aqueous model of table 1. These values are least preferred because computed calcium concentrations during dissolution are greater than the observed values (see footnote to table 1).

*** Estimated log K computed from pH and phase composition at P_{CO_2} = 0.92 atm using the aqueous model of table 1. Computed calcium concentrations during dissolution are in agreement with the measured values (see footnote to table 1).

† Estimated log K computed from pH and phase composition at P_{CO_2} = 0.97 atm using the aqueous model of table 1 but assuming the absence of the $CaHCO_3^+$ species. Computed calcium concentrations during dissolution are in agreement with the observed values (see footnote to table 1).

†† These numbers have been computed from log K† values using $\Delta G°_{f(Ca^{++})}$ = −132.30 kcal/mole, $\Delta G°_{f(Mg^{++})}$ = −108.70 kcal/mole (Parker, Wagman, and Evans, 1971), and $\Delta G°_{f(CO_3^{--})}$ = −126.170 kcal/mole (Wagman and others, 1968).

£ Computed assuming $\mu_{MCO_3}°$ in the computed equilibrium solution is equal to $\mu_{MCO_3(s)}$ in solid solution. Although the trends shown are correct, the absolute values of activities in solid solution are quite sensitive to the $\mu°$ values for $CaCO_3°$, $CaCO_3(s)$, $MgCO_3°$, and $MgCO_3(s)$. See the text for the data used in the calculations.

‡ Extrapolation of dissolution pH to infinite time on $t^{-1/2}$ plots.

§ Computed from the steady state pH data of Chave and others (1962).

Parker, Wagman, and Evans (1971) and for CO_3^{--} of Wagman and others (1968) (table 3).

The molal Gibbs free energy of mixing as a function of mole fraction of $MgCO_3$ in the solid solution has been computed (table 3). These data are compared with the estimates of Lerman (1965) (which were computed from high temperature Mg–calcite stability relations) and values computed from the "steady state" pH data of Chave and others (1962) in figure 12. The values computed by Lerman (1965) are less (that is more stable) than those computed from the data of Chave and others

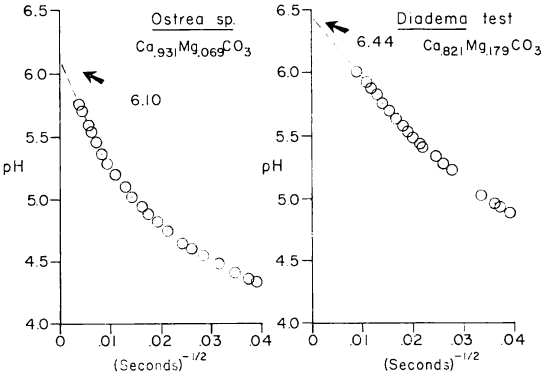

Fig. 10. Linear extrapolation of pH during the dissolution of *Ostrea sp.* and *Diadema* test to infinite time on $t^{-1/2}$ plots to estimate the congruent equilibrium pH. The slopes are approximately linear as time gets large leaving little uncertainty in the predicted equilibrium pH.

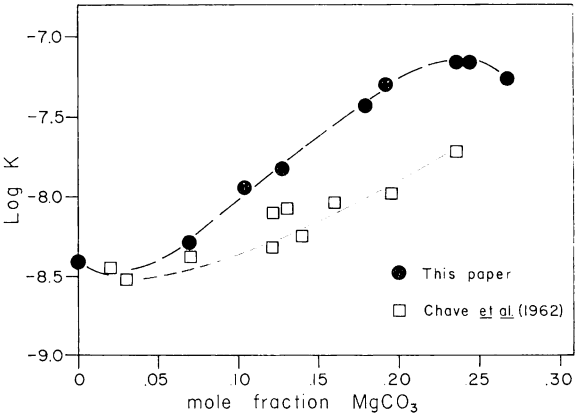

Fig. 11. Comparison of log K data obtained from $t^{-1/2}$ plots with the steady state pH measurements of Chave and others (1962) as a function of mole fraction $MgCO_3$ in calcite. Log K values obtained from $t^{-1/2}$ plots are maximum estimates of the true log K. Because the steady state pH values of Chave and others (1962) correspond to stage 2 in the reaction, equilibrium constants computed from these data are less than the actual values.

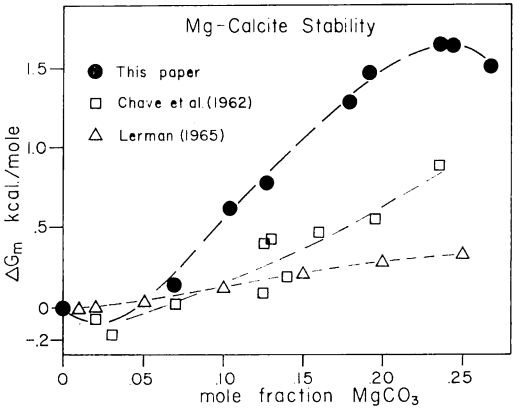

Fig. 12. Comparison of the molal Gibbs free energy of mixing computed from $t^{-1/2}$ plot data with estimates of Lerman (1965) and values computed from the steady state pH data of Chave and others (1962). The values computed from the data of Chave and others (1962) indicate that the most stable calcite contains 2 to 3 mole percent $MgCO_3$. Estimates of ΔG_m from $t^{-1/2}$ plots indicate that magnesian calcite stability passes through a minimum at about 24 mole percent $MgCO_3$.

(1962). All the data of Chave and others (1962) show that Mg–calcites are more stable than computed values from inverse time plots. Lerman's calculated ΔG_m values are more positive (less stable) between 0 and 5 mole percent $MgCO_3$ and more negative beyond 5 mole percent $MgCO_3$ when compared with the values of ΔG_m derived from $t^{-1/2}$ plots. The data computed from $t^{-1/2}$ plots demonstrate that there is a large positive excess free energy in the solid solution. The shape of the G-X curve supports the conclusions of Barnes and O'Neil (1971) that a complete range of calcite solid solution exists between $CaCO_3$ and $Ca_{0.5}Mg_{0.5}CO_3$.

Because the chemical potential of the i^{th} component in phase I (μ_i^{I}) is equal to the chemical potential of the i^{th} component in phase II, that is,

$$\mu_i^{I} = \mu_i^{II} \tag{10}$$

when phase I and phase II are in equilibrium, and, using the relationship

$$\mu_i = \mu_i^{\circ} + RT \ln a_i, \tag{11}$$

it is possible to compute the activities (a_i) of $MgCO_3$ and $CaCO_3$ in solid solution. The activity of $CaCO_3$ in solid solution ($a_{CaCO_3(s)}$) is

$$a_{CaCO_3(s)} = \exp\left(\frac{\mu^{\circ}_{CaCO_3^{\circ}} - \mu^{\circ}_{CaCO_3\ (s)}}{RT} + \ln a_{CaCO_3^{\circ}}\right) \tag{12}$$

where $\mu^{\circ}_{CaCO_3^{\circ}}$ is the ΔG_f° of $CaCO_3^{\circ}$, $\mu^{\circ}_{CaCO_3\ (s)}$ is the ΔG_f° of pure calcite, and $a_{CaCO_3^{\circ}}$ is the activity of the aqueous species $CaCO_3^{\circ}$ in the

computed equilibrium solution. The activity of $MgCO_3$ in solid solution ($a_{MgCO_3\ (s)}$) is

$$a_{MgCO_3\ (s)} = \exp\left(\frac{\mu^\circ_{MgCO_3^\circ} - \mu^\circ_{MgCO_3\ (s)}}{RT} + \ln a_{MgCO_3^\circ}\right) \quad (13)$$

where $\mu^\circ_{MgCO_3}$ is the ΔG_f° of $MgCO_3^\circ$, $\mu^\circ_{MgCO_3\ (s)}$ is the ΔG_f° of pure magnesite, and $a_{MgCO_3^\circ}$ is the activity of the aqueous species $MgCO_3^\circ$ in the computed equilibrium solution.

Activities of $CaCO_3$ and $MgCO_3$ in magnesian calcites, computed from equations (12) and (13) using activities of neutral species computed in the aqueous model and assuming $\mu^\circ_{CaCO_3^\circ} = -262.70$ kcal/mole (compatible with Lafon (ms) and the data of Parker, Wagman, and Evans, 1971), $\mu^\circ_{CaCO_3\ (s)} = -269.94$ kcal/mole (computed from our estimate of calcite pK, 8.412, and the data of Parker, Wagman, and Evans, 1971), $\mu^\circ_{MgCO_3^\circ} = -239.51$ kcal/mole (computed from the data of Lafon, ms, and Parker, Wagman, and Evans, 1971), and $\mu^\circ_{MgCO_3\ (s)} = -246.118$ (Christ and Hostetler, 1970) are shown in table 3. The computed activities of $CaCO_3$ and $MgCO_3$ in magnesium calcites show a tendency toward formation of a stable phase around 2 to 3 mole percent $MgCO_3$ in solid solution (table 3). Large positive departures from ideal mixing above 3 mole percent $MgCO_3$ further demonstrate the metastability of magnesian calcites.

APPLICATION TO THE STABILIZATION OF CARBONATE SEDIMENTS

The data obtained for the dissolution of magnesian calcites suggest that the stabilization of Mg–calcite skeletal grains in carbonate sediments should proceed in a stepwise manner with the most soluble part dissolving first. The measured reaction path for the incongruent dissolution of *Amphiroa r.* shows that the process probably proceeds at saturation or supersaturation with respect to calcite in most carbonate environments. The incongruent dissolution of the most soluble discrete patches of Mg–calcite within a single grain accounts, in part, for the unique preservation of skeletal framework of certain species in ancient rocks.

The stability data suggest that magnesite or dolomite(?) would precipitate in the early diagenesis of carbonate sediments before the waters would contain enough magnesium for a metastable high Mg–calcite–calcite equilibrium. The absence of magnesite in fresh water carbonate diagenetic environments suggests that residence times are short enough, or that the reactions are slow enough, to maintain non-equilibrium relations for the overall incongruent reaction during the stepwise process. As lower Mg–calcites begin to dissolve in the diagenetic process, the Mg^{++} concentration in the ground waters may be sufficient to maintain a metastable equilibrium between the dissolving Mg–calcite and calcite, or a steady state in which Mg–calcite dissolves at calcite saturation or supersaturation.

The log activity ratios of Mg^{++}/Ca^{++} in equilibrium (metastable equilibrium in most cases) with calcite ($CaCO_3$) and magnesium calcites

between 0 and 30 mole percent $MgCO_3$ in solid solution have been computed from the equilibrium

$$Ca_xMg_{(1-x)}CO_3 + (1-x)Ca^{++} = CaCO_3 + (1-x)Mg^{++} \qquad (14)$$

and presented in figure 13. Activity ratios of Mg^{++}/Ca^{++} greater than 2 are uncommon in recent fresh water diagenetic environments and, when found, are usually the result of sea water mixing with meteoric waters and not the result of incongruent dissolution (Plummer and others, in preparation). Therefore, it would be a rare event if equilibrium were reached in the early diagenesis of carbonate sediments. The data of Back and Hanshaw (1970) indicate that many of the waters from the Yucatan and central Florida are near equilibrium with calcite. Their Mg^{++}/Ca^{++} ratios show that the most soluble magnesian calcite that could be in equilibrium with calcite in these waters is about 5 mole percent $MgCO_3$ (fig. 13).

SUMMARY AND CONCLUSIONS

A procedure, first used by Garrels, Thompson, and Siever (1960) for predicting mineral solubility from rate data, is developed, and its limitations defined through controlled experiments on the dissolution of Iceland spar. It is shown that if the surface area to volume ratio is adjusted such that the time to half saturation is greater than or equal to 10 to 12 hours, and kinetic mechanisms of surface reactions do not change, linear extrapolation to infinite time of $t^{-1/2}$ plots should predict the congruent solubility.

This procedure is applied to the dissolution of Mg–calcites and to determining their solubility as a function of the mole fraction of

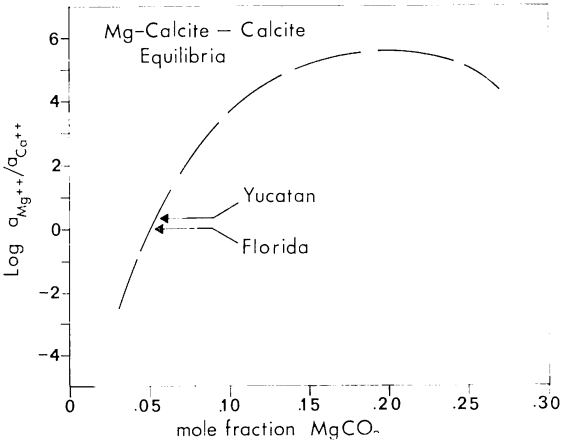

Fig. 13. Activity ratios of magnesium ion to calcium ion in solutions at equilibrium with calcite and magnesium calcites containing 0 to 27 mole percent $MgCO_3$ at 25°C and 1 atm pressure. The range of the activity ratio for central Florida and Yucatan, computed from the data of Back and Hanshaw (1970), are low, suggesting that early diagenesis of carbonate sediments is a nonequilibrium process.

magnesium in the solid solution. The data show that the most stable Mg–calcite contains about 2 mole percent $MgCO_3$. There is a miscibility gap in the G-X curve, and the least stable Mg–calcite contains about 24 mole percent $MgCO_3$. It has long been recognized that there are differences in Mg–calcite solubility, and these differences have now been quantified.

The dissolution characteristics of biogenic Mg–calcites have been studied in detail. Three reaction stages are recognized in closed, isothermal systems at 0.97 atm CO_2. The first corresponds to the congruent dissolution of the most soluble Mg–calcite within the multi-modal skeletal material. The reaction is incongruent to a low Mg–calcite in the second stage and incongruent to both a low Mg–calcite and approximately 12 mole percent $MgCO_3$ calcite in stage 3. The rate of increase of calcium and magnesium follow parabolic rate laws in stage 2, but calcium does not obey a parabolic rate law in stage 3 as calcium is removed from the bulk solution and precipitation takes place within the product layer. The increase of magnesium in the bulk solution follows a parabolic rate law in stage 3 as well.

The dissolution data suggest that the stabilization of carbonate sediments should proceed in a stepwise manner, replacing the most soluble portions within single magnesium calcite skeletal fragments. Calculations show that it is unlikely that metastable equilibria between calcite and Mg–calcites are obtained during the early diagenesis of carbonate sediments.

ACKNOWLEDGMENTS

We are particularly grateful to R. M. Garrels, A. Lerman, O. P. Bricker, and R. C. Speed for interest and stimulating discussions during the research. We benefited significantly from criticism of an earlier version of this manuscript by R. M. Garrels, A. Lerman, R. A. Berner, and Bruce H. T. Chai. We also profited from discussions with B. F. Jones, R. A. Berner, D. C. Thorstenson, and K. Badiozamani at various stages of the research. We thank R. J. Williams for making available to us his interesting work on the dissolution of magnesium calcites.

This research was supported, in part, by funds from Northwestern University, Union Oil Company, National Science Foundation Grant GA-32120, and the Defense Advanced Research Projects Agency, monitored by the U.S. Geological Survey under Order no. 1813, Amendment no. 1. Contribution no. 578, Bermuda Biological Station for Research, St. George's West, Bermuda.

REFERENCES

Back, W., and Hanshaw, B. B., 1970, Comparison of chemical hydrogeology of the carbonate peninsulas of Florida and Yucatan: Jour. Hydrogeology, v. 10, p. 330-368.

Barnes, Ivan, and O'Neil, J. R., 1971, Calcium–magnesium carbonate solid solutions from Holocene conglomerate cements and travertines in the Coast Range of California: Geochim. et Cosmochim. Acta, v. 35, p. 699-718.

Bircumshaw, L. L., and Riddiford, A. C., 1952, Transport control in heterogeneous reactions: Chem. Soc. London Quart. Rev., v. 6, p. 157-185.

Bricker, O. P., 1965, Some stability relations in the system MnO_2–H_2O at 25°C and one atmosphere total pressure: Am. Mineralogist, v. 50, p. 1296-1354.

Butler, J. N., 1964, Ionic Equilibria, a Mathematical Approach: Reading Mass., Addison-Wesley, 547 p.

Chave, K. E., Deffeyes, K. S., Weyl, P. K., Garrels, R. M., and Thompson, M. E., 1962, Observations on the solubility of skeletal carbonates in aqueous solutions: Science, v. 137, p. 33-34.

Christ, C. L., and Hostetler, P. B., 1970, Studies in the system MgO–SiO_2–CO_2–H_2O (II): The activity-product of magnesite: Am. Jour. Sci., v. 268, p. 439-453.

Crank, J., 1956, The Mathematics of Diffusion: Oxford, U. K., Oxford Univ. Press, 347 p.

Garrels, R. M., Thompson, M. E., and Siever, R., 1960, Stability of some carbonates at 25°C and one atmosphere total pressure: Am. Jour. Sci., v. 258, p. 402-418.

Goldsmith, J. R., and Heard, H. C., 1961, Subsolidus phase relations in the system $CaCO_3$–$MgCO_3$: Jour. Geology, v. 69, p. 45-74.

Goldsmith, J. R., Graf, D. L., and Heard, H. C., 1961, Lattice constants of the calcium–magnesium carbonates: Am. Mineralogist, v. 46, p. 453-457.

Greenwald, I., 1941, The dissociation of calcium and magnesium carbonates: Jour. Biol. Chemistry, v. 141, p. 789-796.

Harned, H. S., and Davis, R., Jr., 1943, The ionization constant of carbonic acid in water and the solubility of carbon dioxide in water and aqueous salt solutions from 0 to 50°: Am. Chem. Soc. Jour., v. 65, p. 2030-2037.

Harned, H. S., and Scholes, S. R., Jr., 1941, The ionization constant HCO_3^- from 0 to 50°: Am. Chem. Soc. Jour., v. 63, p. 1706-1709.

Helgeson, H. C., 1967, Solution chemistry and metamorphism, *in* Abelson, P. H., ed., Researches in Geochemistry, v. 2: New York, John Wiley & Sons, p. 362-404.

———— 1969, Thermodynamics of hydrothermal systems at elevated temperatures and pressures: Am. Jour. Sci., v. 267, p. 729-804.

———— 1971, Kinetics of mass transfer among silicates and aqueous solutions: Geochim. et Cosmochim. Acta, v. 35, p. 421-469.

Jost, W., 1952, Diffusion in Solids, Liquids, Gases: New York, Academic Press, 558 p.

Kittrick, J. A., 1966, The free energy of formation of gibbsite and $Al(OH)_4^-$ from solubility measurements: Soil Sci. Soc. America Proc., v. 30, p. 595-598.

Lafon, G. M., ms, 1969, Some quantitative aspects of the chemical evolution of the oceans: Ph.D. dissert., Northwestern Univ., Evanston, Ill.

———— 1970, Calcium complexing with carbonate ion in aqueous solutions at 25°C and 1 atmosphere: Geochim. et Cosmochim. Acta, v. 34, p. 935-940.

Land, L. S., 1967, Diagenesis of skeletal carbonates: Jour. Sed. Petrology, v. 37, p. 914-930.

Langmuir, D., 1968, Stability of calcite based on aqueous solubility measurements: Geochim. et Cosmochim. Acta, v. 32, p. 835-851.

Lerman, A., 1965, Paleoecological problems of Mg and Sr in biogenic calcites in light of recent thermodynamic data: Geochim. et Cosmochim. Acta, v. 29, p. 977-1002.

Luce, R. W., Bartlett, R. W., and Parks, G. A., 1972, Dissolution kinetics of magnesium silicates: Geochim. et Cosmochim. Acta, v. 36, p. 35-50.

Milliman, J. D., Gastner, M., and Muller, J., 1971, Utilization of magnesium in coralline algae: Geol. Soc. America Bull., v. 82, p. 573-580.

Moberly, R., Jr., 1968, Comparison of magnesium calcites of algae and pelecypods by electron microprobe analysis: Sedimentology, v. 11, p. 61-82.

———— 1970, Microprobe study of diagenesis in calcareous algae: Sedimentology, v. 14, p. 113-123.

Morse, J. W., and Berner, R. A., 1972, Dissolution kinetics of calcium carbonate in sea water: II. A kinetic origin for the lysocline: Am. Jour. Sci., v. 272, p. 840-851.

Nakayama, F. S., 1968, Calcium activity, complex and ion-pair in saturated $CaCO_3$ solutions: Soil Sci., v. 106, p. 429-434.

Parker, V. B., Wagman, D. D., and Evans, W. H., 1971, Selected values of chemical thermodynamic properties, Part 6: Natl. Bur. Standards Tech. Note 270-6, 106 p.

Plummer, L. N., ms, 1972, Rates of mineral-aqueous solution reactions: Ph.D. dissert., Northwestern Univ., Evanston, Ill.

———— in preparation, A kinetic model for the dissolution of calcite in CO_2 saturated solutions at 25°C and one atmosphere total pressure: submitted to Geochim. et Cosmochim. Acta.

Plummer, L. N., Mackenzie, F. T., Vacher, H. L., Bricker, O. P., and Land, L. S., in preparation, Geology and geochemistry of Bermuda ground waters: to be submitted to Geol. Soc. America.

Robie, R. A., and Waldbaum, D. R., 1968, Thermodynamic properties of minerals and related substances at 298.15°K (25°C) and one atmosphere (1.013 Bars) pressure and at higher temperatures: U.S. Geol. Survey Bull. 1259, 256 p.

Routson, R. C., and Kittrick, J. A., 1971, Illite Solubility: Soil Sci. Soc. America Proc., v. 35, p. 714-718.

Schmalz, R. F., 1965, Brucite in carbonate secreted by the red algae *Goniolithon sp.*: Science, v. 149, p. 993-996.

Schroeder, J. H., Dwornik, E. J., and Papike, J. J., 1969, Primary protodolomite in Echinoid skeletons: Geol. Soc. America Bull., v. 80, p. 1613-1616.

Stumm, Werner, and Morgan, J. J., 1970, Aquatic Chemistry: New York, Wiley Intersci., 583 p.

Wagman, D. D., Evans, W. H., Parker, V. B., Halow, I., Bailey, S. M., and Schumm, R. H., 1968, Selected values of chemical thermodynamic properties, Part 3: Natl. Bur. Standards Tech. Note 270-3, 264 p.

Weaver, R. M., Jackson, M. L., and Syers, J. K., 1971, Magnesium and silicon activities in matrix solutions of montmorillonite-containing soils in relation to clay mineral stability: Soil Sci. Soc. America Proc., v. 35, p. 823-830.

Weber, J. N., and Kaufman, J. W., 1965, Brucite in the calcareous algae *Goniolithon*: Science, v. 149, p. 996-997.

Winland, H. D., 1969, Stability of calcium carbonate polymorphs in warm, shallow seawater: Jour. Sed. Petrology, v. 39, p. 1579-1587.

Wollast, R., 1967, Kinetics of the alteration of K-feldspar in buffered solutions at low temperature: Geochim. et Cosmochim. Acta, v. 31, p. 635-648.

———— 1971, Kinetic aspects of the nucleation and growth of calcite from aqueous solutions, *in* Bricker, O. P., ed., Carbonate Cements: Baltimore, Md., Johns Hopkins Univ. Press, p. 264-273.